The Astrophysical Journal Letters, 901:L39 (9pp), 2020 October 1 https://doi.org/10.3847/2041-8213/abb5b5

The Origin of Inequality: Isolated Formation of a 30+10 $M_\odot$ Binary Black Hole Merger

A. Olejak[1], M. Fishbach[2], K. Belczynski[1], D. E. Holz[2], J.-P. Lasota[1,3], M. C. Miller[4], and T. Bulik[5]
[1] Nicolaus Copernicus Astronomical Center, Polish Academy of Sciences, ul. Bartycka 18, 00-716 Warsaw, Poland; aleksandra.olejak@wp.pl
[2] Enrico Fermi Institute, Department of Physics, Department of Astronomy & Astrophysics, KICP, University of Chicago, Chicago, IL 60637, USA
[3] Institut d'Astrophysique de Paris, CNRS et Sorbonne Université, UMR 7095, 98bis Bd Arago, F-75014 Paris, France
[4] Department of Astronomy and Joint Space-Science Institute, University of Maryland, College Park, MD 20742−2421, USA
[5] Astronomical Observatory, Warsaw University, Al. Ujazdowskie 4, 00-478 Warsaw, Poland
Received 2020 July 20; revised 2020 September 3; accepted 2020 September 5; published 2020 October 2

Abstract

The LIGO/Virgo Collaboration has reported the detection of GW190412, a black hole–black hole (BH–BH) merger with the most unequal masses to date. (Another system, with even more unequal-mass components, was recently published by LIGO/Virgo: GW190814 ($m_1 = 23\ M_\odot$, $m_2 = 2.6\ M_\odot$); however, it is not known whether it is a BH–BH or BH–NS merger (Abbott et al. 2020).) They are $m_1 = 24.4$–$34.7\ M_\odot$ and $m_2 = 7.4$–$10.1\ M_\odot$, corresponding to a mass ratio of $q = 0.21$–0.41 (90% probability range). Additionally, GW190412's effective spin was estimated to be $\chi_{\rm eff} = 0.14$–0.34, with the spin of the primary BH in the range $a_{\rm spin} = 0.17$–0.59. Based on this and prior detections, $\gtrsim$10% of BH–BH mergers have $q \lesssim 0.4$. Major BH–BH formation channels (i.e., dynamics in dense stellar systems, classical isolated binary evolution, or chemically homogeneous evolution) tend to produce BH–BH mergers with comparable masses (typically with $q \gtrsim 0.5$). Here we test whether the classical isolated binary evolution channel can produce mergers resembling GW190412. We show that our standard binary evolution scenario, with the typical assumptions on input physics that we have used in the past, produces such mergers. For this particular model of the input physics the overall BH–BH merger rate density in the local universe ($z \sim 0$) is 73.5 Gpc^{-3} yr^{-1}, while for systems with $q < 0.41$ the rate density is 6.8 Gpc^{-3} yr^{-1}. The results from our standard model are consistent with the masses and spins of the black holes in GW190412, as well as with the LIGO/Virgo estimate of the fraction of unequal-mass BH–BH mergers. As GW190412 shows some weak evidence for misaligned spins, we provide distribution of the precession parameter in our models and conclude that if among the new LIGO/Virgo detections the evidence of system precession is strong and more than 10% of BH–BH mergers have large in-plane spin components ($\chi_{\rm p} > 0.5$), then the common envelope isolated binary BH–BH formation channel can be excluded as their origin.

Unified Astronomy Thesaurus concepts: Black hole physics (159); High energy astrophysics (739); Black holes (162); Stellar evolution (1599); Stellar evolutionary models (2046); Compact objects (288); Common envelope binary stars (2156); Gravitational wave sources (677)

1. Introduction

The first confirmed double black hole (BH–BH) coalescence to be reported from the LIGO/Virgo O3 run, GW190412, differs from all previously announced BH–BH mergers in one important detail: it is the first BH–BH detection that has a mass ratio inconsistent with unity (The LIGO Scientific Collaboration & the Virgo Collaboration 2020). All 10 BH–BH mergers announced by the LIGO/Virgo team from the O1 and O2 observational campaigns were consistent with being equal-mass mergers (Abbott et al. 2019a, 2019b; Fishbach & Holz 2020). In contrast, GW190412's component masses are $m_1 = 29.7^{+5.0}_{-5.3}\ M_\odot$ and $m_2 = 8.4^{+1.7}_{-1.0}\ M_\odot$, with a mass ratio of $q = 0.28^{+0.13}_{-0.07}$ (median and 90% symmetric credible interval) and a maximum mass ratio of $q = 0.59$ (99% probability). The dimensionless spin of the primary (more massive) BH spin is estimated to be $a_{\rm spin1} = 0.17$–0.59. The LIGO/Virgo Collaboration also gave their constraints on the system effective spin parameter, which is expressed by the formula

$$\chi_{\rm eff} = \frac{m_1 a_{\rm spin1} \cos\theta_1 + m_2 a_{\rm spin2} \cos\theta_2}{m_1 + m_2} \quad (1)$$

where θ_i is the angle between the individual BH spin $a_{\rm spini}$ and the system orbital angular momentum. The estimated value of the system effective spin parameter is $\chi_{\rm eff} = 0.25^{+0.08}_{-0.11}$ (90% probability). The inferred BH–BH merger rate density from O1/O2 is 9.7–101 Gpc^{-3} yr^{-1}. From this and previous detections, $\gtrsim$10% of BH–BH mergers have mass ratios $q < 0.40$ (The LIGO Scientific Collaboration & the Virgo Collaboration 2020).

It is expected that merging BH–BH systems may form through several channels. These include the classical isolated binary evolution channel (Bond & Carr 1984; Tutukov & Yungelson 1993; Lipunov et al. 1997; Voss & Tauris 2003; Belczynski et al. 2010b, 2016b; Dominik et al. 2012; Kinugawa et al. 2014; Eldridge & Stanway 2016; Hartwig et al. 2016; Spera et al. 2016; Woosley 2016; Stevenson et al. 2017; Hainich et al. 2018; Kruckow et al. 2018; Marchant et al. 2019; Spera et al. 2019; Bavera et al. 2020), the dense stellar system dynamical channel (Portegies Zwart & McMillan 2000; Miller & Hamilton 2002a, 2002b; Gültekin et al. 2004, 2006; Portegies Zwart et al. 2004; O'Leary et al. 2007; Sadowski et al. 2008; Downing et al. 2010; Antonini & Perets 2012; Benacquista & Downing 2013; Bae et al. 2014; Chatterjee et al. 2017; Hurley et al. 2016; Mapelli 2016; Rodriguez et al. 2016, 2018; VanLandingham et al. 2016; Arca-Sedda & Capuzzo-Dolcetta 2019; Askar et al. 2017; Samsing 2018; Banerjee 2018; Morawski et al. 2018; Di Carlo et al. 2019; Perna et al. 2019; Zevin et al. 2019; Kremer et al. 2020), isolated multiple (triple, quadruple) systems (Antonini et al. 2017; Silsbee & Tremaine 2017;

Arca-Sedda et al. 2018; Liu & Lai 2018; Fragione & Kocsis 2019), mergers of binaries in galactic nuclei (Antonini & Perets 2012; Hamers et al. 2018; Hoang et al. 2018; Fragione et al. 2019), and the chemically homogeneous evolution channel consisting of rapidly spinning stars in isolated binaries (de Mink & Mandel 2016; Mandel & de Mink 2016; Marchant et al. 2016; du Buisson et al. 2020).

In those formation scenarios BH–BH systems typically form with comparable mass components ($q \gtrsim 0.5$). These predictions are challenged by GW190412.

In this study we demonstrate that in the isolated binary channel a small but significant fraction of systems lead to a BH–BH merger similar to GW190412. We provide a proof-of-principle example of an isolated binary that is both qualitatively and quantitatively indistinguishable from GW190412. We emphasize that we have implemented only one model, incorporating our best estimates of the physics and astrophysics that set the evolution of stars in binary systems. We leave to future work a more extensive study, investigating a greater parameter space and exploring model uncertainties. Our results, when combined and contrasted with similar studies of other formation channels, suggest a plausible origin for GW190412.

2. Calculations

We use the population synthesis code StarTrack (Belczynski et al. 2002, 2008a) to test the possibility of the formation of a BH–BH merger resembling GW190412. We employ the rapid core-collapse supernova (SN) engine neutron star (NS)/BH mass calculation (Fryer et al. 2012), with weak mass loss from pulsational pair instability SNe (Belczynski et al. 2016a). We assume standard wind losses for massive stars: O/B star (Vink et al. 2001) winds and luminous blue variable (LBV) winds (specific prescriptions for these winds are listed in Section 2.2 of Belczynski et al. 2010a). BH natal spins are calculated under the assumption that angular momentum in massive stars is transported by the Tayler–Spruit magnetic dynamo as adopted in the MESA stellar evolutionary code (Spruit 2002). Such BH natal spins are at the level of $a_{\rm spin} \sim 0.1$ (see Belczynski et al. 2020) and may be overridden if the immediate BH progenitor (Wolf–Rayet (WR)) stars in close binaries (orbital periods $P_{\rm orb} < 1.3$ days) are subject to tidal interactions. In such cases we employ the scheme described in Section 2.5 of Belczynski et al. (2020). For BH–WR, WR–BH and WR–WR binary systems with orbital periods in the range $P_{\rm orb} = 0.1$–1.3 days the BH natal spin magnitude is fit from WR star spun-up MESA models (see Equation (15) of Belczynski et al. 2020), while for systems with $P_{\rm orb} < 0.1$ day the BH spin is equal to 1.0. BH spins may be increased by accretion in binary systems. We treat accretion onto a compact object during Roche lobe overflow (RLOF) and from stellar winds using the analytic approximations presented in King et al. (2001) and Mondal et al. (2020). We adopted limited 5% Bondi accretion rate onto BHs during the common envelope (CE) phase (Ricker & Taam 2008; MacLeod & Ramirez-Ruiz 2015; MacLeod et al. 2017). The estimate of Bondi accretion rate during the CE phase is derived in Appendix B.

The most updated description of StarTrack is given in Belczynski et al. (2020). Here we use input physics from model M30 of that paper except for two important differences: First, instead of using the initial mass ratio distribution from Sana et al. (2012), which allows only $q = 0.1$–1.0, we now extend this distribution to lower mass ratios $q = q_{\rm min}$–1.0, where $q_{\rm min}$ is chosen in such a way that a star mass is allowed to reach the hydrogen burning limit $M_{\rm ZAMS} = 0.08\,M_\odot$. Second, for cases in which we do not know whether we should apply thermal timescale RLOF or CE for systems with NS/BH accretors, we use a specific diagnostic diagram to decide between thermal RLOF and CE (see Section 5.2 of Belczynski et al. 2008a). In this single step of binary evolution we previously applied our older numerical approximation of the calculation of accretion onto NS/BH presented in Belczynski et al. (2008b) instead of our newly adopted analytic approach (King et al. 2001; Mondal et al. 2020). These two changes increase the estimated total BH–BH merger rate in the local universe ($z \sim 0$) from 43.7 $\rm Gpc^{-3}\,yr^{-1}$ (model M30.B; Belczynski et al. 2020) to 73.5 $\rm Gpc^{-3}\,yr^{-1}$ (this study; see below).

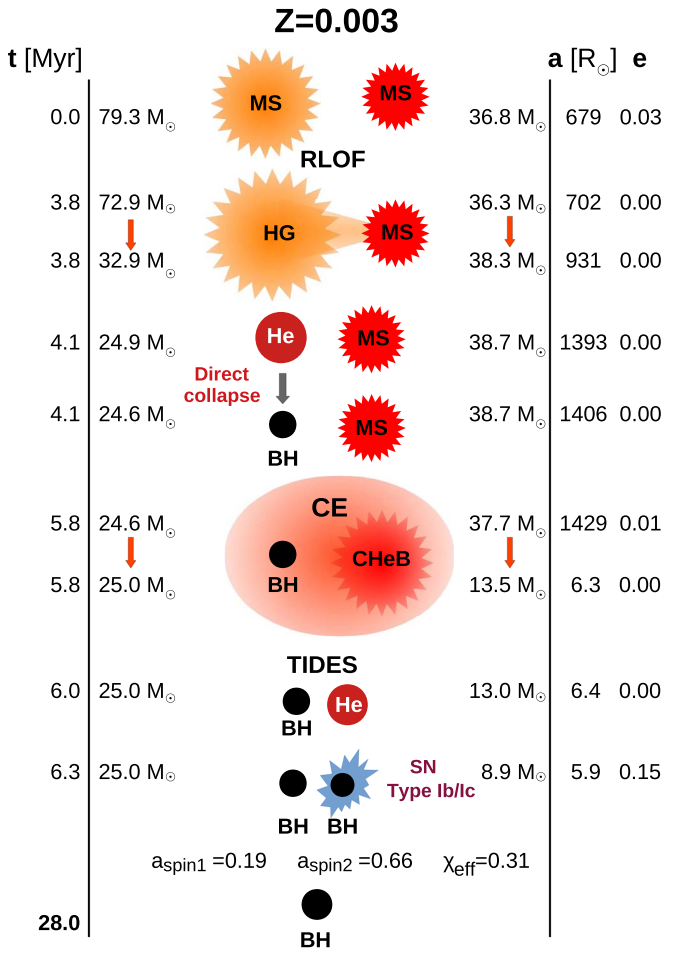

Figure 1. Evolution of an isolated binary system that produces a BH–BH merger resembling GW190412 (see Section 3 for details). MS: main sequence star, HG: Hertzsprung gap star, CHeB: core helium-burning star, He: naked helium star, BH: black hole, RLOF: Roche lobe overflow, CE: common envelope.

3. Example of Evolution

In Figure 1 we present an example of the evolution of a binary system that leads to the formation of close BH–BH systems consistent with the parameters estimated for GW190412. This system was picked from the most populated formation channel of BH–BH mergers with $q < 0.41$ (see Table 1). This system has both BH masses and primary BH spin $a_{\rm spin1}$ within the range of 90% uncertainties given by The

Table 1
Evolutionary Channels for $q < 0.41$ BH–BH Mergers

No.	Evolutionary History[a]	$\mathcal{R}_1$[b]	$\mathcal{R}_2$[c]	$\mathcal{R}_3$[d]	$\mathcal{R}_4$[e]
1	RLOF1 BH1 CE2 BH2	5.90	0.49	0.11	0.11
2	RLOF1 BH1 RLOF2 CE2 BH2	0.76	0.04	0.01	0.01
3	RLOF1 BH1 CE2 RLOF2 BH2	0.02	0.01	0.00	0.00
4	OTHER CHANNELS	0.11	0.00	0.01	0.00
	All	6.79	0.54	0.13	0.11

Notes.
[a] RLOF: stable Roche lobe overflow, CE: common envelope, BH: black hole formation, 1: indicates primary (initially more massive star), 2: secondary star being donor in RLOF or CE.
[b] Merger rate density ($\mathrm{Gpc^{-3}\ yr^{-1}}$) for systems with $q < 0.41$.
[c] Above and $24.4 < m_1/M_\odot < 34.7$ and $7.4 < m_2/M_\odot < 10.1$.
[d] Above and $0.17 < a_{\mathrm{spin,a}} < 0.59$.
[e] Above and $0.14 < \chi_{\mathrm{eff}} < 0.34$.

LIGO Scientific Collaboration & the Virgo Collaboration (2020).

This system, with initial primary mass $\sim 79\ M_\odot$ and secondary mass $\sim 37\ M_\odot$, is formed in a low-metallicity environment $Z = 0.003$ ($\sim 0.1\ Z_\odot$) with an initial separation of $a \sim 680\ R_\odot$ and eccentricity $e \sim 0.03$. When the more massive star leaves the main sequence, the system circularizes ($e = 0.0$) at the onset of the stable RLOF phase, during which the donor (primary star) loses a significant amount (over 50%) of its mass. After finishing its nuclear evolution, the primary undergoes direct collapse and forms a first BH with no natal kick and no associated SN explosion. After the secondary leaves the main sequence and becomes a core helium-burning giant, the system enters a CE phase during which the secondary loses its H-rich envelope. The system separation decreases to only $a \sim 6\ R_\odot$. After CE, the secondary is a massive naked helium WR star. The binary separation is so small that the secondary is subject to strong tidal interactions and is spun up. At time $t = 6.3$ Myr since the start of the evolution, the secondary explodes as a Type Ib/c SN (mass ejection of $\sim 3.0\ M_\odot$; 3D natal kick of $v_{\mathrm{kick}} = 98\ \mathrm{km\ s^{-1}}$) and forms a second BH. Due to the small orbital separation, the two BHs, now with a mass ratio of $q = 0.36$, merge in just ~ 21.7 Myr.

The first BH forms with a spin $a_{\mathrm{spin1}} = 0.13$ (calculated from MESA single stellar models with Spruit 1999 angular momentum transport; see Figure 2 of Belczynski et al. 2020) that is perfectly aligned with the binary angular momentum ($\theta_1 = 0$ deg). Had we adopted more efficient angular momentum transport in stars (Fuller & Ma 2019; Fuller et al. 2019; Ma & Fuller 2019) than employed in the standard MESA then primary BH spin would change to $a_{\mathrm{spin1}} \sim 0.01$. This BH accretes in CE and during stable RLOF from its companion ($\sim 0.4\ M_\odot$) and increases its spin to $a_{\mathrm{spin1}} = 0.19$. The second, lower mass, BH forms with spin $a_{\mathrm{spin2}} = 0.66$ that is slightly misaligned by its natal kick to $\theta_2 = 5$ deg. The spin magnitude is obtained from rapidly spinning MESA naked helium star models with spins that correspond to a tidally locked star for a given orbital period in our binary models (see Equation (15) of Belczynski et al. 2020). The effective spin parameter of this BH–BH merger is $\chi_{\mathrm{eff}} = 0.31$, within the LIGO/Virgo range for GW190412 (0.14–0.34). It is noted that, for the virtually aligned geometry of BH spins with binary angular momentum in this example, we do not expect any precession. Yet, there seems to be marginal evidence for precession in GW190412.

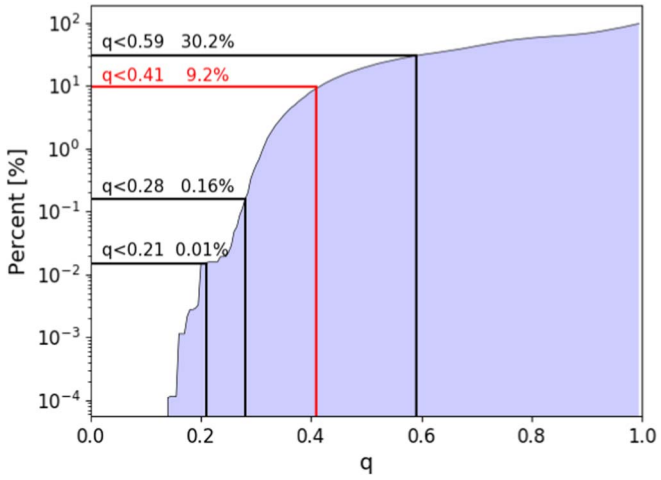

Figure 2. Cumulative fraction of merging BH–BH systems with mass ratio smaller than q in the local universe ($z \sim 0$). Fractions for selected mass ratios $q < 0.21$ (0.01%), $q < 0.28$ (0.16%), and $q < 0.59$ (30.2%) are marked with black lines. The red line marks $q < 0.41$, indicating that 9.2% of our simulated binary mergers at $z \sim 0$ are consistent with the 90% upper limit on q for GW190412.

We provide a discussion of precession in Section 5 and Appendix A.

One might be tempted to identify phase 4 (just before CE in Figure 1) of the evolution of our binary system with high-mass X-ray binaries of the Cyg X-1 type ($M_{\mathrm{BH}} = 14.8\ M_\odot$, O star companion $M_{\mathrm{O}} = 19.2\ M_\odot$ and orbital period of $P_{\mathrm{orb}} = 5.6$ days;[6] this corresponds to a semimajor axis of $a = 43\ R_\odot$). However, Cyg X-1 is an active system (it accretes from a wind), which implies an orbital separation that is too tight to allow survival of the subsequent CE phase (Belczynski et al. 2012). If it instead undergoes a stable RLOF (Pavlovskii & Ivanova 2015; Pavlovskii et al. 2017) then the orbit will widen beyond the limit ($a \sim 50\ R_\odot$) for two BHs to merge within a Hubble time. We note that BH–BH progenitors in our simulations are initially very wide ($a \gtrsim 1000\ R_\odot$) binaries so they can successfully survive the CE phase (de Mink & Belczynski 2015).

4. Population of Low-q BH–BH Mergers

Our simulation results in a $z \sim 0$ population of merging BH–BH systems with a local rate density of $\mathcal{R}_0 = 73.5\ \mathrm{Gpc^{-3}\ yr^{-1}}$. The cumulative distribution of mass ratios for these mergers is presented in Figure 2. In this model the majority of BH–BH mergers ($\sim 80\%$) have large mass ratios ($q > 0.5$), consistent with previous results (Belczynski et al. 2016b). Here we focus on the tail of the distribution extending to more extreme mass ratios. Our model predicts very few systems with mass ratios smaller than the average value reported for GW190412: 0.16% of binaries have $q < 0.28$. However, we report a more significant fraction of systems with mass ratios smaller than the 90% upper bound on GW190412: 9.2% at $q < 0.41$. This fraction becomes significantly higher for the 99% upper bound on GW190412: 30.2% at $q < 0.59$.

In Table 1 we show evolutionary sequences that lead to the formation of BH–BH mergers with small mass ratios: $q < 0.41$. We list the merger rate density arising for typical evolutionary sequences. These are $z \sim 0$ rate densities and are

[6] https://universeathome.pl/universe/black holes.php

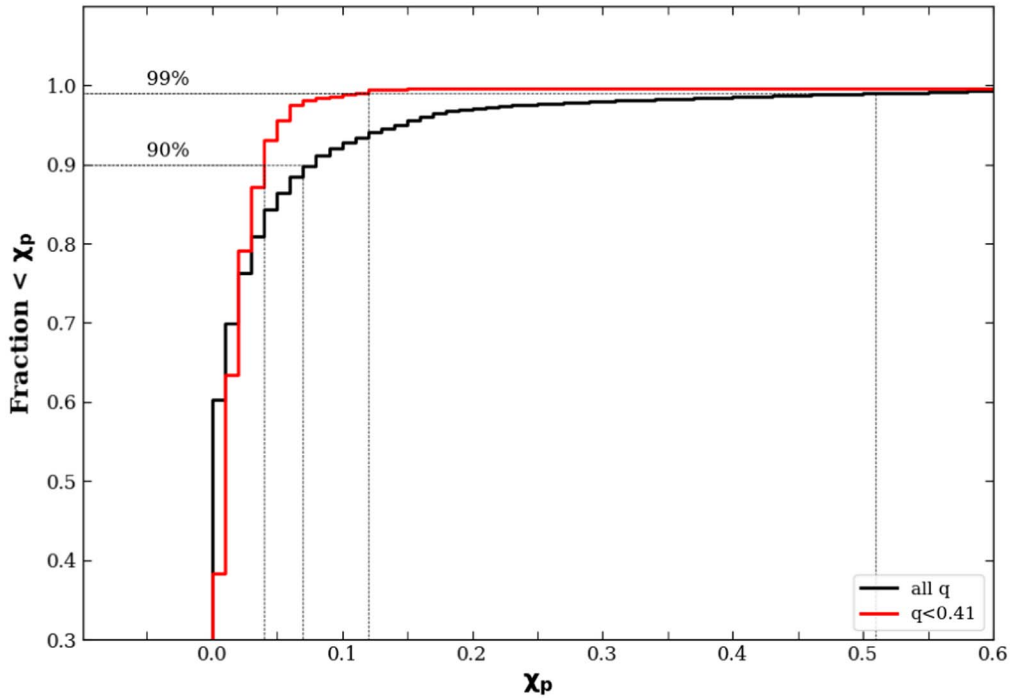

Figure 3. Cumulative distribution of precession parameter χ_p of BH–BH mergers in the local universe ($z \sim 0$). Black line—overall BH–BH population; red line—subpopulation of BH–BH mergers with mass ratio $q < 0.41$. Results for standard model: Spruit–Tayler BH spins + natal kicks lowered by fallback and partial tidal interactions.

subpopulations of the overall local BH–BH merger population ($\mathcal{R}_0 = 73.5\ \mathrm{Gpc^{-3}\ yr^{-1}}$). The table presents merger rate densities for BH–BH systems that are increasingly constrained to resemble GW190412:

1. $\mathcal{R}_1$: $q < 0.41$,
2. $\mathcal{R}_2$: $q < 0.41$ and $24.4 < m_1/M_\odot < 34.7$ and $7.4 < m_2/M_\odot < 10.1$,
3. $\mathcal{R}_3$: $q < 0.41$ and $24.4 < m_1/M_\odot < 34.7$ and $7.4 < m_2/M_\odot < 10.1$ and $0.17 < a_{\mathrm{spin,a}} < 0.59$,
4. $\mathcal{R}_4$: $q < 0.41$ and $24.4 < m_1/M_\odot < 34.7$ and $7.4 < m_2/M_\odot < 10.1$ and $0.17 < a_{\mathrm{spin,a}} < 0.59$ and $0.14 < \chi_{\mathrm{eff}} < 0.34$.

The overall rate of systems with $q < 0.41$ is $\mathcal{R}_1 = 6.8\ \mathrm{Gpc^{-3}\ yr^{-1}}$, which corresponds to ~10% of our overall predicted local merger rate density of BH–BH systems ($\mathcal{R}_0 = 73.5\ \mathrm{Gpc^{-3}\ yr^{-1}}$). This is consistent with the LIGO/Virgo estimate of the fraction of low-mass ratio systems as inferred from the detection of GW190412 combined with previous detections. We emphasize that Figure 2 shows the distribution of the mass ratios for *all* merging binaries in the local universe, which may be different from the distribution of *detected* binaries because it does not incorporate gravitational-wave (GW) selection effects. This is not expected to lead to a significant effect in the case of mass ratio distributions (e.g., see Figure 4 of Fishbach & Holz 2020). In addition, it is to be noted that the LIGO/Virgo estimate of $\gtrsim$10% of binaries having $q \lesssim 0.4$ (The LIGO Scientific Collaboration & the Virgo Collaboration 2020) is for the true (intrinsic) population, not the detected population. This estimate is thus directly comparable to the results from Figure 2.

To produce a low-mass ratio system with a primary BH as massive as 30 $M_\odot$, a progenitor binary needs to have (i) one very massive component ($M_{\mathrm{ZAMS}} \gtrsim 70\ M_\odot$), and (ii) rather low initial stellar mass ratio ($q_{\mathrm{ZAMS}} < 0.5$). In addition, the progenitor binary needs to have low metallicity $Z \lesssim 10\%\ Z_\odot$ ($\lesssim$0.002; Belczynski et al. 2010a). These systems are uncommon, leading to a dearth of small mass ratio BH–BH mergers such as GW190412.

5. Discussion and Conclusions

The existence of unequal-mass binary BHs is to be expected within the isolated binary evolution formation scenario. The mass ratios of such systems were initially investigated by Bulik et al. (2004). They found that in the standard scenario one expects BH–BH systems with high mass ratios above 0.7 to dominate; however, varying the efficiency of the CE evolution phase leads to the formation of systems with mass ratios less than 0.5. Although our knowledge of binary evolution and BH–BH formation has subsequently improved, this result appears robust and remains valid. Dominik et al. (2012) have shown the distribution of mass ratios of BH–BH systems in their Figure 9. They find that for subsolar metallicity a significant fraction of these mergers have mass ratio less than 0.5. An additional hint for the existence of unequal-mass BH–BH systems from isolated binary evolution comes from the analysis of the future evolution of Cyg X-3 (Belczynski et al. 2013). This system will lead to formation of either a BH–NS or BH–BH binary; in the latter case, the mass ratio is expected to be below 0.6. Systems with BH masses similar to GW190412 are also found in results from isolated binary evolution calculations by other groups (e.g., see Figure 5 of Eldridge & Stanway 2016).

The formation channel of GW190412 was considered by Di Carlo et al. (2020, p. 8) both through dynamical formation in open clusters and through the classical isolated binary evolution channel as discussed here. That group finds that systems like GW190412: "can be matched only by dynamical BH–BH born from metal-poor progenitors, because isolated

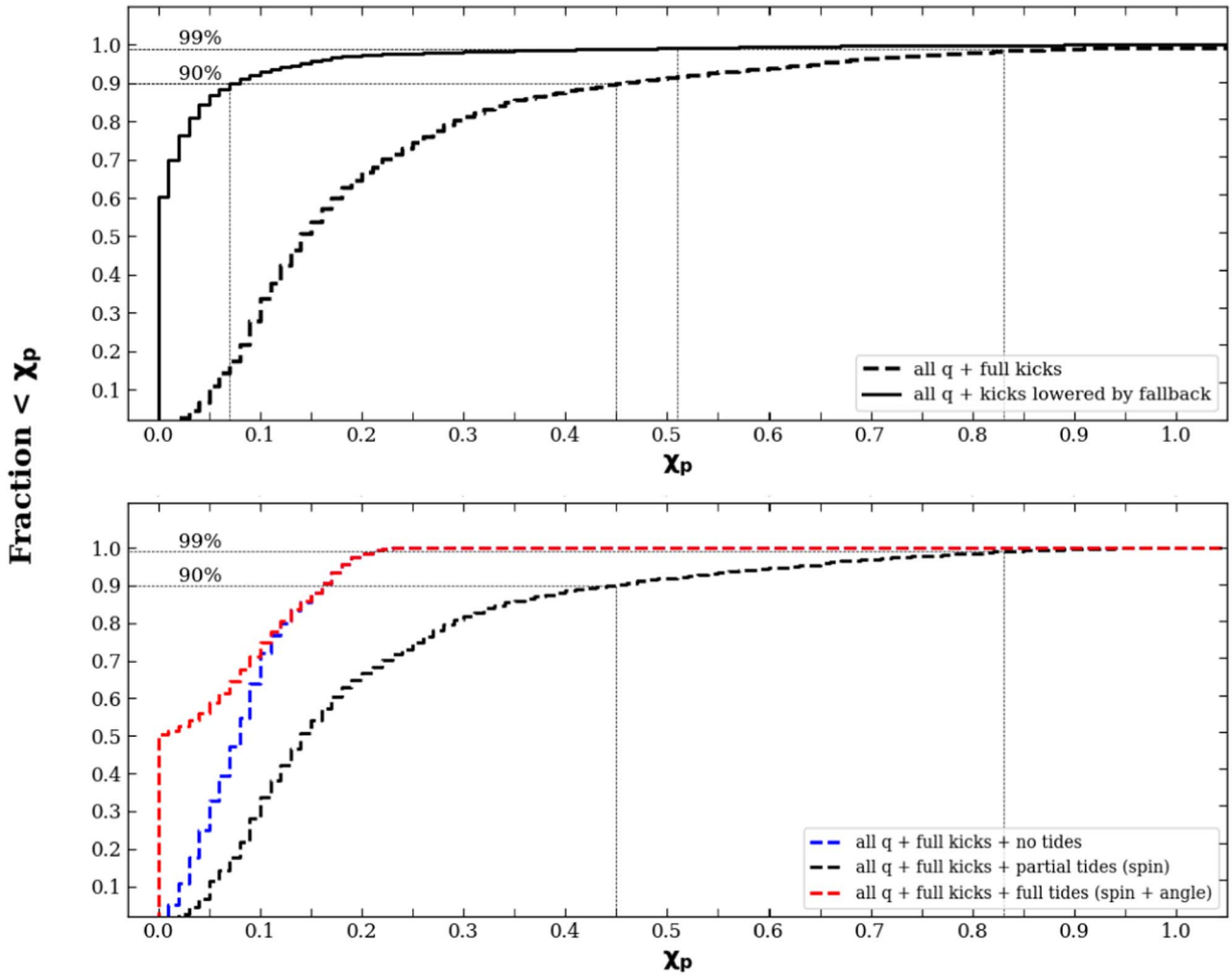

Figure 4. Cumulative distribution of precession parameter χ_p of BH–BH mergers in the local universe ($z \sim 0$). Top panel: solid black line—overall BH–BH population with standard natal kicks lowered by fallback; dashed black line—overall BH–BH population with full natal kicks. Bottom panel: blue dashed line—overall BH–BH population with full natal kicks and no tidal interactions on WR stars; black dashed line—overall BH–BH population with full natal kicks and partial tidal interactions on WR stars (spin magnitude); red dashed line—overall BH–BH population with full natal kicks and full tidal interactions on WR stars (spin magnitude and angles).

binaries can hardly account for its mass ratio in our models." Unlike them, we find that systems like GW190412 are naturally formed by isolated binaries in a small but significant fraction of systems. Note also that the model that we use to account for the formation of GW190412 has also been used to explain the merger rates, masses, and low effective spins of the full O1/O2 LIGO/Virgo BH–BH merger sample (Belczynski et al. 2020).

Mandel & Fragos (2020) have questioned the LIGO/Virgo conclusion that the non-negligible positive effective spin parameter for GW190412 has its origin from a moderate/high spin of the primary (more massive) BH in GW190412 ($a_{\rm spin1} = 0.17 - 0.59$). Instead, Mandel & Fragos (2020) point out that in the classical isolated binary evolution scenario some second-born BHs may form from tidally spun-up helium stars, and that the resulting BHs are expected to have high spins. Using priors consistent with this, they perform an alternate analysis of GW190412, which finds that the primary BH has negligible spin ($a_{\rm spin1} \sim 0$) while the secondary BH has high spin ($a_{\rm spin2} = 0.64 - 0.99$). This possibility is also consistent with our results: we find that in ∼30% of local BH–BH mergers with $q < 0.41$, tidal interactions are strong enough to produce a lower mass BH with spin $a_{\rm spin2} > 0.64$. For example, in Figure 1 we show a system that forms a very close ($a \sim 4\ R_\odot$) binary with a BH and a naked helium star (this is the evolutionary phase just prior BH–BH formation). This naked helium star is subject to tidal spin-up, and instead of forming a slowly spinning BH, it forms a rapidly spinning BH ($a_{\rm spin2} = 0.66$). However, in contrast with Mandel & Fragos (2020) we do not assume that the primary BH spin is negligible. Instead, we calculate the natal BH spins (if not affected by tides) from single stellar models allow for spin increase due to accretion during binary mass transfer phases (see Section 2). The primary BH spins are found to be small, but not negligible. For the case shown in Figure 1, the natal primary BH spin is $a_{\rm spin1} = 0.11$ and then it is increased to $a_{\rm spin1} = 0.19$ through accretion in a CE event. Because both spins are closely aligned with the binary angular momentum (the secondary is slightly misaligned due to a small natal kick, to $\theta_2 = 5$ deg), the effective spin parameter of this system is $\chi_{\rm eff} = 0.31$, which is consistent with the upper end of the LIGO/Virgo 90% probability estimate for GW190412.

GW190412 shows some weak evidence for misaligned spins, with a non-zero precession parameter: $\chi_p = 0.15$–0.49 (90% credible limits). In this system, the amount of observed

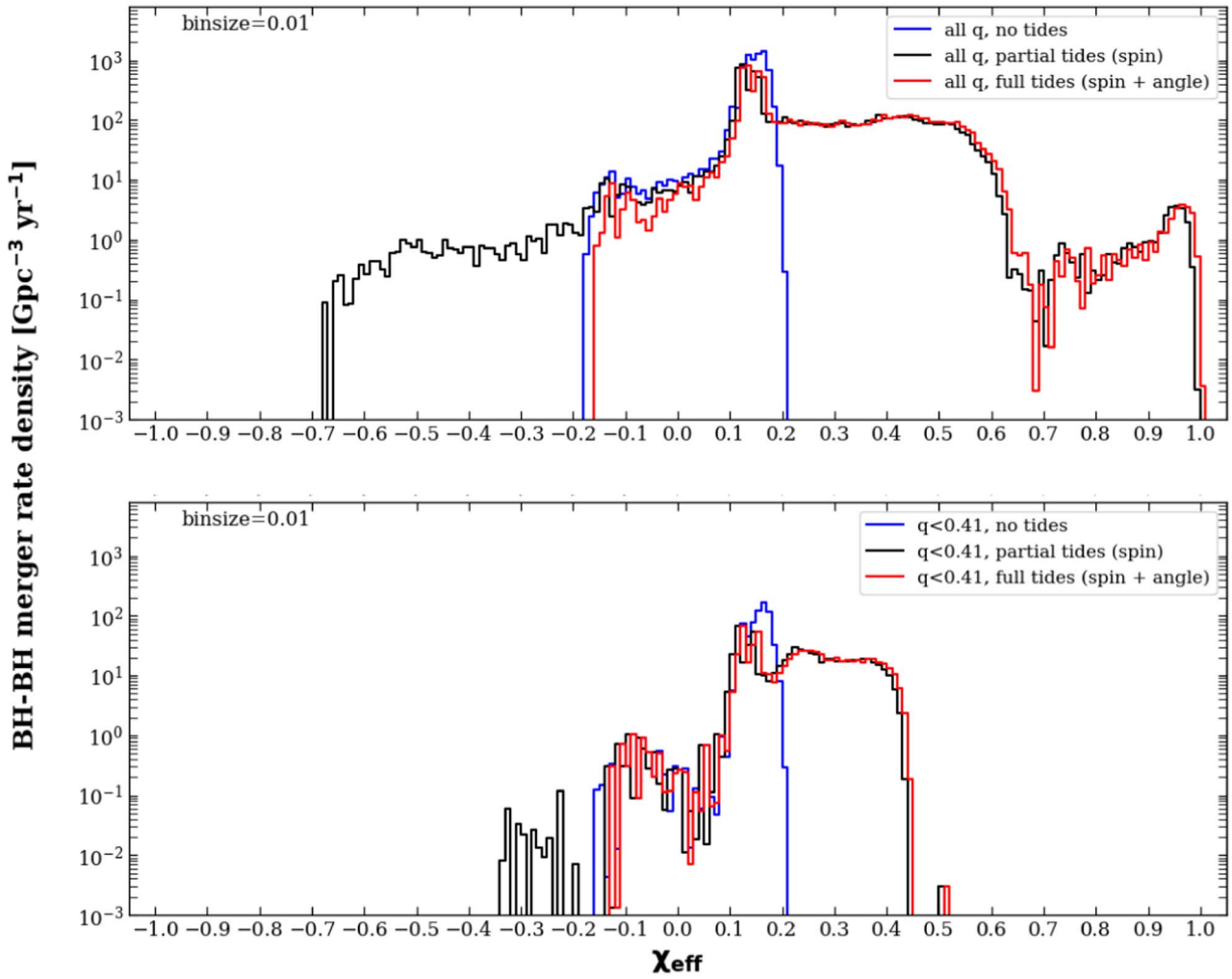

Figure 5. Distribution of effective spin parameter $\chi_{\rm eff}$ of BH–BH mergers in the local universe ($z \sim 0$) for different approaches to tides: blue line—no tides; black line—partial tides; red line—full tides. Top panel: overall BH–BH population. Bottom panel: sub-population of BH–BH mergers with mass ratio $q < 0.41$. Results for standard model: Spruit–Tayler BH spins + natal kicks lowered by fallback.

precession is consistent with noise (see Figure 6 of The LIGO Scientific Collaboration & the Virgo Collaboration 2020), and the mild preference for $\chi_p > 0$ disappears when the GW data is re-analyzed with different priors on the spin magnitudes (Zevin et al. 2020). Nevertheless, it is interesting to explore whether a clear observation of precession would be consistent with our models. In our evolutionary example (see Figure 1) we do not expect to produce any precessing systems as both BHs are almost fully aligned with the binary angular momentum. Some degree of misalignment would appear in our model if, for example, we added a larger natal kick at the formation of the second BH. At this point the binary is so tight that even a large kick would have only a small chance to disrupt this binary. The small natal kick applied to the second BH formed through partial fallback results from the simple assumption that natal kicks scale inversely with the amount of the fallback (Fryer et al. 2012) but little is known about BH natal kicks (Repetto & Nelemans 2015; Belczynski et al. 2016c; Mandel 2016; Repetto et al. 2017; Gandhi et al. 2020). We have estimated the precession parameter for all the BH–BH mergers produced by our model (see Appendix A). The cumulative distribution of $\chi_{\rm p}$ (Figure 3) shows that BH–BH mergers are dominated by low precession parameter values for our standard model (small natal BH kicks). We calculated several additional models adopting high BH natal kicks, and a different approach to tidal spin-up of BH progenitors to be able to provide exclusion statements. If an analysis of the LIGO/Virgo BH–BH population finds that more than 10% of BH–BH mergers have large in-plane spin components ($\chi_{\rm p} > 0.5$), then a CE isolated binary BH–BH formation channel can be excluded as their origin. This conclusion is valid if (i) stars in binaries are born with aligned spins, and (ii) angular momentum transport in massive stars is efficient (driven by magnetic dynamo) producing low natal BH spins ($a_{\rm spin} < 0.2$), unless BH progenitor stars are subject to tidal spin-up. Furthermore, this conclusion is independent of the BH natal kick model or the action of tides on WR stars in close binaries. A similar statement can be made for possible future signals from highly mass asymmetric BH–BH systems with large $\chi_{\rm eff} \gtrsim 0.5$. We show distributions of effective spin parameter for the overall local BH–BH mergers and the low-mass ratio BH–BH sub-population (Figure 5). This figure indicates that the effective spin values for low-q sub-population are systematically smaller and limited to $|\chi_{\rm eff}| \leqslant 0.5$.

We have shown that the isolated classical binary evolution channel can form binaries similar to GW190412. This is an

important explicit proof-of-principle demonstration that the event GW190412 may be the result of isolated evolution. Furthermore, Figure 2 shows that the detection of a binary with a mass ratio of $q \lesssim 0.4$ is to be expected within the current GW sample, because this sub-population constitutes ∼10% of the total population. We find that, if GW190412 formed via the classical isolated binary channel, it likely evolved from a low-metallicity ($Z < 10\%\ Z_{\odot}$) progenitor system with initial mass ratio $q < 0.5$ between the two massive stars, but that otherwise the system followed an evolutionary path that is typical of the majority of BH–BH mergers (Belczynski et al. 2016b). Over the coming years the population of GW BH–BH mergers is expected to grow to many hundreds of detections. These will facilitate detailed population studies, including a determination of the distribution of mass ratios. While the existing population of BH–BH mergers can be explained using classical isolated binary evolution, the discovery of a large population of binaries with mass ratio $q < 0.2$ would pose a significant challenge to our models.

We would like to thank the anonymous referee for their useful comments. K.B. and A.O. acknowledge support from the Polish National Science Center (NCN) grant Maestro (2018/30/A/ST9/00050). J.P.L. was supported in part by the French Space Agency CNES. T.B. was supported by TEAM/2016-3/19 grant from FNP. D.E.H. was supported by NSF grant PHY-1708081, as well as the Kavli Institute for Cosmological Physics at the University of Chicago through an endowment from the Kavli Foundation. D.E.H. also gratefully acknowledges support from the Marion and Stuart Rice Award. M.C.M. thanks the Radboud Excellence Initiative for supporting his stay at Radboud University.

Appendix A
Precession Parameter

The LIGO/Virgo Collaboration gave an estimate of the GW190412 precession parameter $\chi_{\rm p}$, which is spin-dependent parameter expressed by the formula (Schmidt et al. 2015; Gerosa et al. 2020):

$$\chi_{\rm p} = \max\left[a_{\rm spin1}\sin\theta_1,\ a_{\rm spin2}\sin\theta_2\frac{q(4q+3)}{(4+3q)}\right]. \qquad (2)$$

The value of $\chi_{\rm p}$ given by LIGO/Virgo is in the range of 0.15–0.49 (90% credible limits). This is unique among the other BH–BH merger detections for which the precession parameter was uninformative, and consistent with $\chi_{\rm p} = 0$ (corresponding to perfectly aligned spins). GW190412 shows weak evidence for precession, we note that the measurement remains inconclusive, and small values of $\chi_{\rm p} < 0.1$ cannot be ruled out (The LIGO Scientific Collaboration & the Virgo Collaboration 2020; Zevin et al. 2020). Although $\chi_{\rm p}$ is poorly measured for individual GW events, combining multiple observations will reveal the population distribution of $\chi_{\rm p}$. This will provide a powerful test of our models, as we discuss below.

We calculated distributions of precession parameter values for our standard model and its several variations.

The cumulative distribution of $\chi_{\rm p}$ for our standard model is shown in Figure 3. For the overall BH–BH population merging at $z \sim 0$ as well as for the low-mass ratio sub-population ($q < 0.41$), the distribution is dominated by low precession parameters values: 90% of overall BH–BH binaries have precession parameter $\chi_{\rm p} < 0.07$ while 99% have $\chi_{\rm p} < 0.51$. Low mass ratio BH–BH mergers have even lower values: 90% of the systems have $\chi_{\rm p} < 0.04$ and 99% have $\chi_{\rm p} < 0.11$. The reason for the difference between those two populations is the relation between natal kicks and the mass of resulting compact object. Less massive BHs usually get higher natal kicks, so precession is more likely in mergers with low-mass BHs. In the low-mass ratio mergers, one of the BHs is always massive, and is formed through direct collapse (without a SN explosion). In contrast, in the overall BH–BH population, there are cases of mergers with two low-mass BHs that may form with high natal kicks. High natal kicks increase the degree of misalignment and subsequently increase $\chi_{\rm p}$.

To test the maximum allowed level of precession in our isolated binary evolution model, we increase BH natal kicks to the high speeds observed for single pulsars in the Galaxy (Maxwellian distribution with $\sigma = 265$ km s^{-1}; Hobbs et al. 2005), and apply these natal kicks to all BHs independent of their mass. In this model, the distribution of precession parameters shifted to higher values, with 90% of all BH–BH mergers (any q) having $\chi_{\rm p} < 0.43$ and 99% having $\chi_{\rm p} < 0.82$ (see top panel of Figure 4). Note that our standard model employs BH natal kicks decreased by fallback, and in practice, massive BHs ($M \gtrsim 10$–$15\ M_{\odot}$) do not receive natal kicks.

We have also tested the effect of tidal interactions between a WR star (an immediate BH progenitor in our models) and its massive companion on precession parameters. Three variants of approach to tides are shown in the bottom panel of Figure 4. Note that tides may change misalignment angles and BH natal spin magnitude affecting the value of $\chi_{\rm p}$. We perform this analysis on high natal BH kick model to maximize the effect of tides. We tested a variant with no tidal interactions on WR stars (no tides), a variant in which tides only affect spin magnitude (partial tides: our standard model approach), and a variant in which tides affect spin magnitude and cause alignment of a WR star with binary angular momentum (full tides; note that this star spin may be misaligned if earlier natal kick on the other star shifted binary angular momentum vector).

We find that among these three drastically different approaches to tides, our standard model (partial tides) may be considered as an upper limit on $\chi_{\rm p}$ parameter value. For both the no-tides and full-tides variants 90% of systems have $\chi_{\rm p} \lesssim 0.2$ while 99% of systems have $\chi_{\rm p} \lesssim 0.15$, which is much less than for the variant with partial tides (for 90% $\chi_{\rm p} < 0.43$ and for 99% $\chi_{\rm p} < 0.82$). The lower limit on $\chi_{\rm p}$ values in the no-tides variant is simply related to the fact that the BH spin magnitudes are not increased due to tidal interactions in the WR phase. In the case of full tides the sharp increase in fraction of systems near $\chi_{\rm p} \sim 0$ is generated due to the assumption about the WR star spin alignment with the system angular momentum so the part of the formula corresponded to a given BH (Equation (2)) takes the value of zero. Those differences cause the removal of systems with high $\chi_{\rm p}$ from the distribution for the no-tides and full-tides variants as contrasted with our partial-tides model.

In Figure 5 we present effective spin $\chi_{\rm eff}$ distribution in our standard model for three different approaches to tides. In the top panel there is a distribution for overall BH–BH population merging at z ∼ 0 and in the bottom panel we show distribution for low-mass ratio sub-population with $q < 0.41$. Adopted

tides approaches gives different results, especially for overall BH–BH population. In the no-tides approach both distributions (overall and low q) are similarly dominated by low effective spin parameter and the absolute value is limited to $|\chi_{\rm eff}| < 0.2$. In the partial-tides and full-tides approaches the possible absolute value of effective spin widens to around $|\chi_{\rm eff}| < 0.5$ for low-mass ratio sub-population while in overall population effective spin may take values up 1.0. This is caused by the fact that for the overall BH–BH population there are more possible evolutionary scenarios in which both objects could be the subject of WR tides.

Based on our results we may conclude that if an analysis of the LIGO/Virgo BH–BH population reveals that more than 10% of systems have high precession ($\chi_{\rm p} \leqslant 0.5$) then the CE isolated binary BH–BH formation channel can be excluded as their origin. This conclusion is valid if (i) stars in binaries are born with aligned spins and (ii) natal BH spins are low ($a_{\rm spin} < 0.2$) unless their progenitor stars are subject to strong tidal interactions, and is independent of the BH natal kick model or the action of tides on WR stars in close binaries. We note that we have assumed in all our simulations that stellar spins are aligned with the binary angular momentum at zero-age main sequence, that only natal kicks at BH formation may misalign stellar/BH spins, and that only tidal interactions can realign stellar spins. A similar statement can be made for possible future signals from highly mass asymmetric BH–BH systems with large $\chi_{\rm eff} \gtrsim 0.5$. Distributions indicates that the effective spin values for low-q sub-population are systematically smaller and limited to $|\chi_{\rm eff}| \leqslant 0.5$.

Appendix B
Accretion during CE Phase

Here we describe the procedure of calculating the accretion rate onto the BH during the CE phases. The procedure is based on Equations (5.3)–(5.7) of Bethe & Brown (1998) and Equations (A1)–(A10) from Belczynski et al. (2002).

In our calculations CE begins once BH companion (CE donor) expands beyond its Roche lobe and mass transfer is determined to proceed on a dynamical timescale (Belczynski et al. 2008a). CE evolution and accretion onto the BH ends when the donor's envelope is ejected and the donor mass is reduced to the mass of its core. We use the following symbols: $M_{\rm A}$—mass of the BH, $M_{\rm B}$—mass of the donor, $M_{\rm B,core}$—mass of the donor's core, A—orbital separation (semimajor axis).

First, we compare energy-loss rate related to the accretion onto the BH and the rate of the orbital energy dissipation due to the dynamical friction of BH in the donor's envelope:

$$\dot{E}_{\rm acc} = -\dot{E}_{\rm orb}. \tag{3}$$

The formula for $\dot{E}_{\rm acc}$ is introduced by Equations (5.3)–(5.7) in Bethe & Brown (1998) and (A1) Belczynski et al. (2002) while $\dot{E}_{\rm orb}$ is expressed by Equation (A2) Belczynski et al. (2002). Note, that $\dot{E}_{\rm acc}$ include mass accretion rate $\dot{M}_{\rm A}$ given by the Bondi–Hoyle–Lyttleton theory. Comparing the time derivatives of both energies we obtain the first time-independent differential equation, which contains $\frac{dM_A}{dM_B}$ and $\frac{dA}{dM_B}$ (Equation (A3) of Belczynski et al. 2002).

Second, we compare the donor's envelope binding energy with the orbital energy, since CE is ejected on the expense of the binary orbital energy with an efficiency described by parameter $\alpha_{\rm CE}$. Formulas for both energies are given by Equations (A4) and (A5) of Belczynski et al. (2002). We then take donor's mass derivative

$$\frac{dE_{\rm bind}}{dM_B} = -\alpha_{\rm CE}\left(\frac{E_{\rm orb}}{dM_B}\right) \tag{4}$$

to obtain the second equation containing $\frac{dM_A}{dM_B}$ and $\frac{dA}{dM_B}$ (Equation (A7) of Belczynski et al. 2002). Therefore, we can rearrange the two above equations to have two ordinary differential equations, one for increasing mass of BH, and one for decreasing orbital separation. We solve them within realistic limits: using donor's envelope mass (CE), which is known (in contrast to integrating over unknown timescale of CE). We integrate from pre-CE donor mass ($M_{\rm B}$) to its post-CE mass ($M_{\rm B,core}$) to obtain the final binary separation and final mass of the accreting BH.

We assume that accretion onto a BH is always set by the Bondi rate (as implemented above). However, we take into account the fact that not entire infalling/accreting mass is actually accumulated onto a BH. Some of the accreting mass is lost before reaching BH (e.g., angular momentum barrier in asymmetric flow around BH (MacLeod & Ramirez-Ruiz 2015), accretion disk winds; see Mondal et al. 2020 and references therein). We allow only some fraction of accreting mass to accumulate into a BH increasing its mass and spin. In particular, we estimate accretion mass $\Delta M_{\rm bondi}$ assuming that accretion proceeds with Bondi rate (i.e., integrating Equation (A9) of Belczynski et al. 2002), and we adopt that only 5% of this mass actually accumulates on the BH ($\Delta M_{\rm accu}$):

$$\Delta M_{\rm accu} = 0.05 \Delta M_{\rm bondi}. \tag{5}$$

ORCID iDs

A. Olejak https://orcid.org/0000-0002-6105-6492
M. Fishbach https://orcid.org/0000-0002-1980-5293
D. E. Holz https://orcid.org/0000-0002-0175-5064
J.-P. Lasota https://orcid.org/0000-0002-6171-8396
M. C. Miller https://orcid.org/0000-0002-2666-728X
T. Bulik https://orcid.org/0000-0003-2045-4803

References

Abbott, B. P., Abbott, R., Abbott, T. D., et al. 2019a, ApJL, 882, L24
Abbott, B. P., Abbott, R., Abbott, T. D., et al. 2019b, PhRvX, 9, 031040
Abbott, R., Abbott, T. D., Abraham, S., et al. 2020, ApJL, 896, L44
Antonini, F., & Perets, H. B. 2012, ApJ, 757, 27
Antonini, F., Toonen, S., & Hamers, A. S. 2017, ApJ, 841, 77
Arca-Sedda, M., & Capuzzo-Dolcetta, R. 2019, MNRAS, 483, 152
Arca-Sedda, M., Li, G., & Kocsis, B. 2018, arXiv:1805.06458
Askar, A., Szkudlarek, M., Gondek-Rosińska, D., Giersz, M., & Bulik, T. 2017, MNRAS, 464, L36
Bae, Y.-B., Kim, C., & Lee, H. M. 2014, MNRAS, 440, 2714
Banerjee, S. 2018, MNRAS, 473, 909
Bavera, S. S., Fragos, T., Qin, Y., et al. 2020, A&A, 635, A97
Belczynski, K., Bulik, T., & Fryer, C. L. 2012, arXiv:1208.2422
Belczynski, K., Bulik, T., Fryer, C. L., et al. 2010a, ApJ, 714, 1217
Belczynski, K., Bulik, T., Mandel, I., et al. 2013, ApJ, 764, 96
Belczynski, K., Dominik, M., Bulik, T., et al. 2010b, ApJL, 715, L138
Belczynski, K., Heger, A., Gladysz, W., et al. 2016a, A&A, 594, A97
Belczynski, K., Holz, D. E., Bulik, T., & O'Shaughnessy, R. 2016b, Natur, 534, 512
Belczynski, K., Kalogera, V., & Bulik, T. 2002, ApJ, 572, 407
Belczynski, K., Kalogera, V., Rasio, F. A., et al. 2008a, ApJS, 174, 223
Belczynski, K., Klencki, J., Fields, C. E., et al. 2020, A&A, 636, A104
Belczynski, K., Repetto, S., Holz, D. E., et al. 2016c, ApJ, 819, 108

Belczynski, K., Taam, R. E., Rantsiou, E., & van der Sluys, M. 2008b, ApJ, 682, 474
Benacquista, M. J., & Downing, J. M. B. 2013, LRR, 16, 4
Bethe, H. A., & Brown, G. E. 1998, ApJ, 506, 780
Bond, J. R., & Carr, B. J. 1984, MNRAS, 207, 585
Bulik, T., Gondek-Rosinska, D., & Belczynski, K. 2004, MNRAS, 352, 1372
Chatterjee, S., Rodriguez, C. L., Kalogera, V., & Rasio, F. A. 2017, ApJL, 836, L26
de Mink, S. E., & Belczynski, K. 2015, ApJ, 814, 58
de Mink, S. E., & Mandel, I. 2016, MNRAS, 460, 3545
Di Carlo, U. N., Giacobbo, N., Mapelli, M., et al. 2019, MNRAS, 487, 2947
Di Carlo, U. N., Mapelli, M., Giacobbo, N., et al. 2020, MNRAS, 498, 495
Dominik, M., Belczynski, K., Fryer, C., et al. 2012, ApJ, 759, 52
Downing, J. M. B., Benacquista, M. J., Giersz, M., & Spurzem, R. 2010, MNRAS, 407, 1946
du Buisson, L., Marchant, P., Podsiadlowski, P., et al. 2020, arXiv:2002.11630
Eldridge, J. J., & Stanway, E. R. 2016, MNRAS, 462, 3302
Fishbach, M., & Holz, D. E. 2020, ApJL, 891, L27
Fragione, G., Grishin, E., Leigh, N. W. C., Perets, H. B., & Perna, R. 2019, MNRAS, 488, 47
Fragione, G., & Kocsis, B. 2019, MNRAS, 486, 4781
Fryer, C. L., Belczynski, K., Wiktorowicz, G., et al. 2012, ApJ, 749, 91
Fuller, J., & Ma, L. 2019, ApJL, 881, L1
Fuller, J., Piro, A. L., & Jermyn, A. S. 2019, MNRAS, 485, 3661
Gandhi, P., Rao, A., Charles, P. A., et al. 2020, MNRAS: Letters, 496, L22
Gerosa, D., Vitale, S., & Berti, E. 2020, PhRvL, 125, 101103
Gültekin, K., Miller, M. C., & Hamilton, D. P. 2004, ApJ, 616, 221
Gültekin, K., Miller, M. C., & Hamilton, D. P. 2006, ApJ, 640, 156
Hainich, R., Oskinova, L. M., Shenar, T., et al. 2018, A&A, 609, A94
Hamers, A. S., Bar-Or, B., Petrovich, C., & Antonini, F. 2018, ApJ, 865, 2
Hartwig, T., Volonteri, M., Bromm, V., et al. 2016, MNRAS, 460, L74
Hoang, B.-M., Naoz, S., Kocsis, B., Rasio, F. A., & Dosopoulou, F. 2018, ApJ, 856, 140
Hobbs, G., Lorimer, D. R., Lyne, A. G., & Kramer, M. 2005, MNRAS, 360, 974
Hurley, J. R., Sippel, A. C., Tout, C. A., & Aarseth, S. J. 2016, PASA, 33, e036
King, A. R., Davies, M. B., Ward, M. J., Fabbiano, G., & Elvis, M. 2001, ApJL, 552, L109
Kinugawa, T., Inayoshi, K., Hotokezaka, K., Nakauchi, D., & Nakamura, T. 2014, MNRAS, 442, 2963
Kremer, K., Ye, C. S., Rui, N. Z., et al. 2020, ApJS, 247, 48
Kruckow, M. U., Tauris, T. M., Langer, N., Kramer, M., & Izzard, R. G. 2018, MNRAS, 481, 1908
Lipunov, V. M., Postnov, K. A., & Prokhorov, M. E. 1997, AstL, 23, 492
Liu, B., & Lai, D. 2018, ApJ, 863, 68
Ma, L., & Fuller, J. 2019, MNRAS, 488, 4338
MacLeod, M., Antoni, A., Murguia-Berthier, A., Macias, P., & Ramirez-Ruiz, E. 2017, ApJ, 838, 56
MacLeod, M., & Ramirez-Ruiz, E. 2015, ApJ, 803, 41
Mandel, I. 2016, MNRAS, 456, 578
Mandel, I., & de Mink, S. E. 2016, MNRAS, 458, 2634
Mandel, I., & Fragos, T. 2020, ApJL, 895, L28
Mapelli, M. 2016, MNRAS, 459, 3432
Marchant, P., Langer, N., Podsiadlowski, P., Tauris, T. M., & Moriya, T. J. 2016, A&A, 588, A50
Marchant, P., Renzo, M., Farmer, R., et al. 2019, ApJ, 882, 36
Miller, M. C., & Hamilton, D. P. 2002a, MNRAS, 330, 232
Miller, M. C., & Hamilton, D. P. 2002b, ApJ, 576, 894
Mondal, S., Belczyński, K., Wiktorowicz, G., Lasota, J.-P., & King, A. R. 2020, MNRAS, 491, 2747
Morawski, J., Giersz, M., Askar, A., & Belczynski, K. 2018, MNRAS, 481, 2168
O'Leary, R. M., O'Shaughnessy, R., & Rasio, F. A. 2007, PhRvD, 76, 061504
Pavlovskii, K., & Ivanova, N. 2015, MNRAS, 449, 4415
Pavlovskii, K., Ivanova, N., Belczynski, K., & Van, K. X. 2017, MNRAS, 465, 2092
Perna, R., Wang, Y.-H., Farr, W. M., Leigh, N., & Cantiello, M. 2019, ApJL, 878, L1
Portegies Zwart, S. F., Baumgardt, H., Hut, P., Makino, J., & McMillan, S. L. W. 2004, Natur, 428, 724
Portegies Zwart, S. F., & McMillan, S. L. W. 2000, ApJL, 528, L17
Repetto, S., Igoshev, A. P., & Nelemans, G. 2017, MNRAS, 467, 298
Repetto, S., & Nelemans, G. 2015, MNRAS, 453, 3341
Ricker, P. M., & Taam, R. E. 2008, ApJL, 672, L41
Rodriguez, C. L., Amaro-Seoane, P., Chatterjee, S., et al. 2018, PhRvD, 98, 123005
Rodriguez, C. L., Haster, C.-J., Chatterjee, S., Kalogera, V., & Rasio, F. A. 2016, ApJL, 824, L8
Sadowski, A., Belczynski, K., Bulik, T., et al. 2008, ApJ, 676, 1162
Samsing, J. 2017, PhRvD, 10, 103014
Sana, H., de Mink, S. E., de Koter, A., et al. 2012, Sci, 337, 444
Schmidt, P., Ohme, F., & Hannam, M. 2015, PhRvD, 91, 024043
Silsbee, K., & Tremaine, S. 2017, ApJ, 836, 39
Spera, M., Giacobbo, N., & Mapelli, M. 2016, MmSAI, 87, 575
Spera, M., Mapelli, M., Giacobbo, N., et al. 2019, MNRAS, 485, 889
Spruit, H. C. 1999, A&A, 349, 189
Spruit, H. C. 2002, A&A, 381, 923
Stevenson, S., Vigna-Gómez, A., Mandel, I., et al. 2017, NatCo, 8, 14906
The LIGO Scientific Collaboration, & the Virgo Collaboration 2020, PhRvD, 102, 043015
Tutukov, A. V., & Yungelson, L. R. 1993, MNRAS, 260, 675
VanLandingham, J. H., Miller, M. C., Hamilton, D. P., & Richardson, D. C. 2016, ApJ, 828, 77
Vink, J. S., de Koter, A., & Lamers, H. J. G. L. M. 2001, A&A, 369, 574
Voss, R., & Tauris, T. M. 2003, MNRAS, 342, 1169
Woosley, S. E. 2016, ApJL, 824, L10
Zevin, M., Berry, C. P. L., Coughlin, S., Chatziioannou, K., & Vitale, S. 2020, ApJL, 899, L17
Zevin, M., Samsing, J., Rodriguez, C., Haster, C.-J., & Ramirez-Ruiz, E. 2019, ApJ, 871, 91